Atmos. Chem. Phys. Discuss., 14, 8819–8850, 2014
www.atmos-chem-phys-discuss.net/14/8819/2014/
doi:10.5194/acpd-14-8819-2014

Atmospheric Chemistry and Physics Discussions

Aqueous-phase photooxidation of levoglucosan – a mechanistic study using Aerosol Time of Flight Chemical Ionization Mass Spectrometry (Aerosol-ToF-CIMS)

R. Zhao, E. L. Mungall, A. K. Y. Lee, D. Aljawhary, and J. P. D. Abbatt

Department of Chemistry, University of Toronto, 80 St. George Street, Toronto, ON, Canada

Received: 19 March 2014 – Accepted: 24 March 2014 – Published: 2 April 2014

Correspondence to: J. P. D. Abbatt (jabbatt@chem.utoronto.ca)

Published by Copernicus Publications on behalf of the European Geosciences Union.

Abstract

Levoglucosan (LG) is a widely employed tracer for biomass burning (BB). Recent studies have shown that LG can react rapidly with hydroxyl (OH) radicals in the aqueous phase, despite many mass balance receptor models assuming it to be inert during atmospheric transport. In the current study, aqueous-phase photooxidation of LG by OH radicals was performed in the laboratory. The reaction kinetics and products were monitored by Aerosol Time of Flight Chemical Ionization Mass Spectrometry (Aerosol-ToF-CIMS). Approximately 50 reaction products were detected by the Aerosol-ToF-CIMS during the photooxidation experiments, representing one of the most detailed product studies yet performed. By following the evolution of mass defects of product peaks, unique trends of adding oxygen (+O) and removing hydrogen (−2H) were observed among the products detected, providing useful information to determine potential reaction mechanisms and sequences. As well, bond scission reactions take place, leading to reaction intermediates with lower carbon numbers. We introduce a data analysis framework where the average oxidation state (OS_c) is plotted against a novel molecular property: double bond equivalence to carbon ratio (DBE / #C). The trajectory of LG photooxidation on this plot suggests formation of poly-carbonyl intermediates and their subsequent conversion to carboxylic acids as a general reaction trend. We also determined the rate constant of LG with OH radicals at room temperature to be $1.08 \pm 0.16 \times 10^9\ M^{-1}\ s^{-1}$. By coupling an Aerosol Mass Spectrometer (AMS) to the system, we observed a rapid decay of the mass fraction of organic signals at mass-to-charge ratio 60 ($f60$), corresponding closely to the LG decay monitored by the Aerosol-ToF-CIMS. The trajectory of LG photooxidation on a $f44$–$f60$ correlation plot matched closely to literature field measurement data. This implies that aqueous-phase photooxidation might be partially contributing to aging of BB particles in the ambient atmosphere.

1 Introduction

Biomass burning (BB) is a major source of atmospheric particles and volatile organic compounds (VOCs). Directly emitted VOCs and primary organic aerosol (POA) are subject to subsequent atmospheric processing, leading to formation of secondary organic aerosol (SOA) (Jimenez et al., 2009). Reliable and quantitative apportionment is required to understand the effects of BB on air quality and climate. Apportionment of BB is commonly done using chemical tracers (Simoneit, 2002). Levoglucosan (LG) is a widely used particle-phase molecular tracer of BB (Simoneit et al., 1999), due to its source-specificity and abundance in BB aerosol.

Traditionally, LG has been considered to be highly stable in the atmosphere (Fraser and Lakshmanan, 2000; Simoneit et al., 2004). Stability is an important requirement for a molecular tracer, as it is a major assumption made in Chemical Mass Balance Receptor Models commonly employed for source apportionment (Schauer et al., 1996; Robinson et al., 2006). However, studies from the past decade have shown that LG is subject to atmospheric loss. For example, the particulate concentration of LG relative to other BB tracers is lower in the summer than in the winter, implying an enhanced photooxidative decay (Saarikoski et al., 2008; Mochida et al., 2010; Zhang et al., 2010). Measurements using Aerosol Mass Spectrometry (AMS) have also demonstrated that the decay of BB organic aerosol signature both in the field and laboratory experiments is accompanied by a decrease in m/z 60 and an increase in m/z 44 (Grieshop et al., 2009; Hennigan et al., 2010; Cubison et al., 2011; Ortega et al., 2013).

The decay of LG can be explained by several pathways. Heterogeneous oxidation of LG by gas-phase oxidants has been studied in the laboratory (Kessler et al., 2010; Hennigan et al., 2010; Knopf et al., 2011), where it has been demonstrated that particle-phase LG can be oxidized by hydroxyl (OH) radicals efficiently, leading to LG lifetimes on the order of days. More recently, gas-phase oxidation has also been proposed to contribute to LG loss (May et al., 2012). A small fraction of particle-phase LG can volatilize into the gas phase where is oxidized efficiently. A third explanation

for the observed LG decay is reactive loss in the aqueous phase, such as cloud water or aqueous aerosol particles. Studies from the past decade have revealed the atmospheric aqueous phase as an important reaction medium where organic compounds can be processed, leading to formation and aging of SOA (Blando and Turpin, 2000; Ervens et al., 2011). BB particles can be hygroscopic, depending on their size and inorganic composition (Petters and Kreidenweis, 2007; Petters et al., 2009), therefore a highly functionalized and water soluble organic species, such as LG, can be subject to aqueous-phase processing. Two laboratory studies have investigated the kinetics of aqueous-phase OH oxidation of LG (Hoffmann et al., 2010; Teraji and Arakaki, 2010), finding that OH is the main sink for LG in the tropospheric aqueous phase with lifetimes on the order of hours. By contrast, little is known of the aqueous-phase reaction mechanism of LG. The only studies are those of Holmes and Petrucci who investigated acid-catalyzed and OH-induced oligomerization (Holmes and Petrucci, 2007, 2006) and a recent theoretical study of possible reaction pathways (Bai et al., 2013).

The primary objective of this work is to provide a detailed mechanistic understanding of this oxidation chemistry, which is needed to incorporate LG photooxidation into cloudwater models and to obtain more insight into the atmospheric processing of BB particles. As well, we revisit the reaction kinetics with OH radicals under conditions relevant to cloudwater processing. Aerosol Time-of-Flight Chemical Ionization Mass Spectrometry (Aerosol-ToF-CIMS) is employed to directly monitor LG and its reaction products in real time, after aerosolization of the reaction solution. The high mass resolution of the Aerosol-ToF-CIMS enables unambiguous determination of product elemental composition, and shed light into fundamental aspects of aqueous-phase photooxidation. We also demonstrate a novel analysis method, utilizing oxidation state (OS_c) and double bond equivalence (DBE), to obtain functional group information. To relate our results to previous field studies of BB aerosol, an AMS is employed to connect the chemistry to changes in the AMS signals at m/z 60 and 44.

2 Experimental methods

2.1 Solution preparation and photooxidation

A solution of LG (1 mM) was prepared weekly by dissolving a commercial source (Sigma Aldrich, 99 %) in milliQ water (18 MΩ-cm; TOC ≤ 2 ppb; ELGA-PURELAB Flex). The reaction solution was prepared prior to each experiment by further diluting the stock solution in a Pyrex bottle to a volume of either 1 L (for the mechanistic study) or 100 mL (for the kinetic study) with a LG concentration of 10 µM for the mechanistic experiments or 30 µM for the kinetic experiments. H_2O_2 (Sigma Aldrich, ≥ 30%, Trace-SELECT) was added to the solution as the precursor of hydroxyl (OH) radicals upon irradiation. The concentration of H_2O_2 was typically 1 mM, unless mentioned otherwise. The reaction solution was placed in a cylindrical photo-reactor (Radionex, RMR-200) which supplies UVB radiation from all the sides, but not from the top or bottom. The solution was constantly stirred by a magnetic stir bar, with a fan employed to minimize solution heating. The solution temperature during photooxidation was approximately 301 K. A series of control experiments was performed to confirm that LG was not directly photolyzed under UVB light. A small amount of LG reacted upon H_2O_2 addition in the dark which did not affect the results.

2.2 Aerosol-ToF-CIMS

The experimental apparatus is illustrated in Fig. 1. During photooxidation, the solution was constantly atomized by a constant output atomizer (TSI, model 3076), using compressed air (BOC Linde, Grade 0.1) as the carrier gas. The particle flow was introduced through Siltek-coated stainless steel tubing (1/4 inch diameter, 70 cm long, VWR) heated to 100 or 150 °C. Organic species in the aqueous droplets evaporate in the heated line and are detected by a Chemical Ionization Mass Spectrometer (CIMS). This method of coupling a heated line to CIMS is referred to as Aerosol-CIMS and was first introduced by Smith and coworkers (Hearn and Smith, 2004), and later employed

to investigate aqueous-phase organic chemistry (Sareen et al., 2010; Zhao et al., 2012; Aljawhary et al., 2013). The strength of Aerosol CIMS lies in the fast time response of CIMS, enabling in-situ monitoring of aqueous-phase chemistry. In the current study, high mass resolution (3000 to 4000 Th Th^{-1} in the relevant m/z range in the V-mode) and excellent detection sensitivity were achieved by employing an Aerodyne High Resolution Time of Flight Chemical Ionization Mass Spectrometer (Bertram et al., 2011). This technique is hereafter referred to as Aerosol-ToF-CIMS. For all the experiments, the ToF-CIMS was operated in the V-mode, and the data were analyzed using Tofwerk v. 2.2. Details on the data analysis are described elsewhere (Aljawhary et al., 2013 and references herein).

Our previous study has shown that Aerosol-ToF-CIMS can be used to target different analyte types through the choice of reagent ion. Three reagent ions were employed in the current study: protonated water clusters ($(H_2O)_nH^+$), iodide water clusters ($I(H_2O)_n^-$) and acetate ($CH_3C(O)O^-$). These reagent ions were generated by introducing water vapor, gas-phase CH_3I, and gas-phase acetic anhydrate, respectively, through a ^{210}Po radioactive cell (NRD, P-2021). The detailed setup, ionization mechanisms and sensitivity of each of these reagent ions for atmospherically relevant organic compounds have been summarized in Aljawhary et al. (2013), and are mentioned only briefly here. $(H_2O)_nH^+$ can detect organic compounds that have higher proton affinity (i.e. higher gas-phase basicity) than that of water clusters ($(H_2O)_n$). $(H_2O)_nH^+$ is employed in the kinetic study because it detects both LG and dimethylsulfoxide (DMSO), the kinetics reference compound (see next section). $I(H_2O)_n^-$ is employed as the primary reagent ion to study reaction mechanisms because it is sensitive to a wide spectrum of oxygenated compounds that can form clusters with I^-, including LG and its reaction products. $CH_3C(O)O^-$ is also employed to study the mechanism and to confirm the results from the $I(H_2O)_n^-$ experiments. $CH_3C(O)O^-$ abstracts a proton from compounds that exhibit higher gas-phase acidity than acetic acid and can selectively detect a variety of organic and inorganic acids. Occasionally non-acid species (e.g. LG) can also form clusters with $CH_3C(O)O^-$.

2.3 Mechanistic and kinetic studies

Investigation of the reaction mechanism focused on the identification of multiple generations of reaction products arising during photooxidation using the $I(H_2O)_n^-$ and $CH_3C(O)O^-$ reagent ions. The rate constant of LG reacting with OH radicals was determined using the relative rate method, where the decay of LG is related to that of DMSO, a reference compound with well-known OH reactivity. A fixed concentration (5 µM) of DMSO (Caledon Laboratory Chemicals, > 99%) was added to the reaction solution prior to the initiation of photooxidation. The signals of LG and DMSO were monitored concurrently using Aerosol-ToF-CIMS with $(H_2O)_nH^+$ as the reagent ion. The following relationship holds for the decay of LG and DMSO:

$$\ln\left(\frac{[\mathrm{LG}]_0}{[\mathrm{LG}]_t}\right) = \frac{k_{\mathrm{LG}}^{\mathrm{II}}}{k_{\mathrm{DMSO}}^{\mathrm{II}}} \times \ln\left(\frac{[\mathrm{DMSO}]_0}{[\mathrm{DMSO}]_t}\right), \quad (1)$$

where $[X]_t$ represents the signal of compound X measured at time t, and k_x^{II} represents the 2nd-order rate constant of X reacting with OH radicals. The relationship in Eq. (1) indicates that plotting $\ln([\mathrm{LG}]_0/[\mathrm{LG}]_t)$ against $\ln([\mathrm{DMSO}]_0/[\mathrm{DMSO}]_t)$ should result in a linear plot, with the slope representing the ratio of the two rate constants.

The LG concentration used (10 to 30 µM) is expected to be similar to cloudwater concentrations, assuming typical organic aerosol loading, LG mass fraction in organic aerosol, and complete scavenging by a typical cloudwater liquid content. We consider the current work a simulation of cloudwater photooxidative processing of LG. Although the H_2O_2 concentration used in the experiment is much higher than the ambient level, the steady state concentration of OH was estimated to be approximately 2×10^{-13} M from the 1st-order decay rate of LG. This steady state concentration of OH radicals is in the range relevant to cloudwater (Jacob, 1986).

2.4 Aerosol Mass Spectrometry (AMS) measurement

In some of the experiments, a fraction of the generated particles was also introduced into an Aerodyne compact time of flight (C-ToF) AMS (Canagaratna et al., 2007) after passing through a diffusion drier (Fig. 1). Previous work in our group has shown that the AMS enables in-situ monitoring of aqueous-phase photooxidation by measuring non-refractory components in the atomized solution (Lee et al., 2011, 2012; Aljawhary et al., 2013). The time resolution of the AMS measurement was 1 min. The data were processed using the AMS data analysis software (Squirrel, version 1.51H for unit mass resolution data) with a corrected air fragment column of the standard fragmentation table (Allan et al., 2004).

3 Results and discussion

3.1 Reaction products and mechanism

Using the $I(H_2O)_n^-$ reagent ion, roughly 50 reaction products were detected as clusters with iodide, as described in the Supplement Table S1. The m/z of the products ranged between 173 Th and 351 Th. While Holmes and Petrucci (2006, 2007) observed significant degree of oligomerization with product m/z up to 1000 Th, oligomers of LG were not observed. The absence of oligomeric products might be due to: (1) the initial concentration of LG being lower in the current study (higher concentrations can facilitate oligomerization (Lim et al., 2010)), (2) the Aerosol-ToF-CIMS set up is not sensitive to oligomers. In fact, the degree of oligomerization was also observed to be minor in our previous study, where glyoxal and methylglyoxal photooxidation was investigated using Aerosol-CIMS (Zhao et al., 2012). Therefore, the current study focuses on discussion of monomeric reaction products.

Overall, the observed products imply that two categories of reaction mechanisms are occurring in the reaction system simultaneously: functionalization and bond-scission.

Functionalization reactions modify the functional groups on the molecules but do not lead to cleavage of carbon-carbon bonds, while bond-scission reactions result in carbon-carbon bond breakage.

3.1.1 Functionalization – unique trends of +O and −2H

LG is detected at m/z 289 as a cluster with iodide ($CH_{10}O_5I^-$). As the LG signal decays, peaks that are a multiple of 16 Th apart from LG (i.e. at m/z 305, 321 and 337) formed rapidly one after another (Fig. 2a). Their elemental compositions are different from each other by an oxygen, and this trend is herein referred to as the "+O" trend. Peaks that are a multiple of 2 Th apart from LG (i.e. m/z 287, 285 and 283) are also observed one after another (Fig. 2b). The elemental composition of these compounds is different by 2 hydrogen atoms from each other, and this trend is referred to as the "−2H" trend hereafter. Interestingly, the +O and the −2H trends proceed simultaneously, forming a series of unique product patterns.

A mass defect plot (Hughey et al., 2001) of the major products detected with the $I(H_2O)_n^-$ reagent ion clearly illustrates the two trends occurring in the system (Fig. 3a). Mass defect diagrams plot mass defect (exact mass – nominal mass) against the exact mass of each compound. Since H atoms and O atoms have their own mass defects (+0.007825 for H and −0.005085 for O), compounds that are apart from each other by 2H line up on a slope of 7.77×10^{-3}, while compounds that are apart by an O line up on a slope of -3.18×10^{-4}, as indicated by the dotted lines in Fig. 3a. The time at which each peak reached its maximum level is used to track the order of formation, and is presented by the color code. It can be clearly seen that multiple +O and −2H trends develop in the reaction system during photooxidation (Fig. 3a). The maximum signal intensity reached by each peak is used as an indicator of the amount of formation and is represented by the area of the data points (in log scale). We note that different compounds exhibit different detection sensitivity to the reagent ion of choice. Aljawhary et al. (2013) have demonstrated that the $I(H_2O)_n^-$ reagent ion can detect oxygenated compounds with three or more carbon number with a relatively constant

detection sensitivity. We consider the signal intensity as a semi-quantitative presentation of the amount of each product.

The +O trend must arise from formation of hydroxyl or hydroperoxyl functional groups because these are the only possible mechanisms leading to addition of oxygen without losing any hydrogen. Formation of these functional groups in the aqueous phase has been well studied (von Sonntag et al., 1997). The reaction is initiated by H-abstraction and formation of an alkylperoxy radical (RO_2). RO_2 can react with another RO_2 or a hydroperoxy radical (HO_2) to form a tetraoxide intermediate which gives rise to a variety of products (Fig. 4, R1 to R3). Among these reaction pathways, R1 gives rise to a hydroxyl functional group. When a tetraoxide is formed between RO_2 and HO_2 radicals (R4), a hydroperoxyl functional group can be generated in analogy to R3. The −2H trend in LG photooxidation has been previously reported by Holmes and Petrucci (2007), likely arising from conversion of hydroxyl functional groups into carbonyl groups (Fig. 4, R5). When the initial H abstraction occurs from a carbon atom with an existing hydroxyl functional group, the subsequently formed peroxy radical leads to formation of a carbonyl group and releases a HO_2 molecule. This study demonstrates that this conversion can occur multiple times, eventually converting a polyol into a poly-carbonyl compound. To confirm this reaction mechanism, we performed an experiment of aqueous-phase photooxidation of another polyol, erythritol, using the same experimental conditions. The same −2H trend was observed, consistent with the proposed reaction mechanism.

The proposed structures of reaction products arising from the +O and −2H trends are included in Fig. 3b which shows a magnified view of the relevant region on the mass defect plot. We note that the mass spectrometric technique employed in the current work does not allow us to unambiguously determine the chemical structures. For example, addition of one hydroperoxyl functional group to a molecule yields the same chemical formula as compared with addition of two hydroxyl functional groups, and our technique cannot distinguish between these two mechanisms. Also, some bond-scission reactions can result in chemicals with the same elemental compositions (see next section). Furthermore, the order in which the hydroxyl groups are converted to

carbonyls is difficult to ascertain. Bai et al. (2013) has demonstrated that H-abstraction at the middle hydroxyl group of LG is energetically favored.

3.1.2 Bond-scission reactions

Scission of C-C bonds is likely triggered by formation of alkoxy radicals via R2 (Fig. 4) from the tetraoxide intermediate. Cleavage of one C-C bond gives rise to an aldehyde and an alkyl radical (R6, Fig. 4). Time series of selected major bond-scission products are shown in Fig. 5a, along with their elemental composition and proposed structures. As a general trend, products with 5 or 6 carbons (i.e. products v, vi, vii) form first, followed by those with smaller carbon numbers as photooxidation proceeds. Using the current mass spectrometric method, it is difficult to unambiguously determine the structure of these detected species. It is also not possible to completely rule out the possibility of the fragmentation of large ions in the mass spectrometer, contributing to peaks with smaller m/z. However, the distinct time profiles observed for most of the products imply that they are independent compounds. The proposed structures have been estimated from a series of reaction mechanisms shown in the Fig. S1. The proposed mechanisms has been constructed based on widely accepted reaction mechanisms, and the sequence of product formation is consistent with the observed time series. The LG photooxidation reaction system is highly complicated, as demonstrated by the proposed mechanisms. Multiple reaction pathways can likely lead to the same product, and one chemical formula may constitute multiple compounds with varying structures. For this reason, the current work is not intended to determine the complete reaction mechanism, but rather to elucidate the general trend of reactions by monitoring major products detected.

We propose that bond-scission may not immediately lead to compounds with fewer carbon numbers in the case of LG photooxidation. This is because LG contains ring structures, and bond scission can likely lead to ring-cleavage before molecule fragmentation. Formation of product vii (Fig. 5a) presents one such example. This bond scission product has a larger molecular weight compared to LG. However, product vii

overlaps with one of the proposed products in the +O and −2H series (see previous sections), making it difficult to elucidate its magnitude of formation. In a study of heterogeneous oxidation of LG and erythritol, Kessler et al. (2010) observed that the mass loss during LG photooxidation was slower than that from erythritol and also proposed that ring-cleavage in the LG system delayed molecule fragmentation. We suspect that this delay might be due to formation of compounds such as product vii.

Formation of small organic acids with carbon numbers equal to or less than two are also observed as later generation products (Fig. 5b), confirmed by both the $I(H_2O)_n^-$ and the $CH_3C(O)O^-$ reagent ion experiments. It is difficult to constrain the explicit formation mechanisms of these small organic acids because they are likely formed from further photooxidation of the many intermediate compounds discussed above. For example, it is well known that glyoxal, which is expected to form as a bond-scission product, forms glyoxylic acid, formic acid, and oxalic acid (Lim et al., 2010; Lee et al., 2011; Zhao et al., 2012). In particular, oxalic acid exhibited continuous formation until the end of the photooxidation (Fig. 5b). This observation agrees with the fact that oxalic acid is relatively unreactive with OH radicals and presents a relatively long-lived reservoir of organic carbon in the aqueous phase. We consider the small organic acids as the final carbon reservoir before they either volatilize from the aqueous phase or are eventually oxidized to CO_2.

3.1.3 Obtaining functional group information from the Aerosol-ToF-CIMS

As a general trend within the LG system, we hypothesize that a series of compounds containing multiple carbonyl functional groups may form as reaction intermediates, and then are subsequently oxidized to carboxylic acids. Carbonyl functional groups have likely arisen from (1) the hydroxyl-to-carbonyl conversion mechanism mentioned in the previous section (R5, Fig. 4), and (2) bond-scission of an alkoxy radical yielding an aldehyde functional group (R6, Fig. 4). Rapid formation of carboxylic acids from aldehydes in the aqueous phase has been well documented (Schuchmann and von Sonntag, 1988; Lim et al., 2010; Zhao et al., 2012). This is a mechanism unique to the aqueous

phase because it is initiated by hydration of an aldehyde or an acyl radical (Scheme 4, Fig. S1).

Although the Aerosol-ToF-CIMS is a powerful tool to elucidate elemental composition, its ability to reveal functional group information is limited. Here, we present an analysis framework employing two molecular properties, double bond equivalence (DBE) (Bateman et al., 2011) and oxidation state (OS_c) (Kroll et al., 2011), which are calculated by Eq. (2) and Eq. (3):

$$DBE = \#C - \frac{\#H}{2} + 1. \quad (2)$$

$$OS_c = 2 \times O/C - H/C. \quad (3)$$

where #C and #H represent the numbers of carbon and hydrogen atoms contained in each product molecule, while O/C and H/C represent the oxygen-to-carbon and hydrogen-to-carbon ratios of each product, respectively. These parameters are readily available from the high mass resolution analysis of the Aerosol-ToF-CIMS. The intensity-weighted average of DBE and OS_c from the 50 products monitored by the $I(H_2O)_n^-$ reagent ion (Table S1) are displayed in Fig. 6. While OS_c exhibited continuous increase throughout the entire photooxidation experiment, DBE exhibited an increase at the beginning, but a decrease in the latter half of the experiment. An increase in DBE can be attributed to formation of (1) carbon-carbon double/triple bonds, (2) ring structures, or (3) carbon-oxygen double bonds (i.e. C=O in carbonyl or carboxylic acid). Under an oxidative environment, formation of (1) and (2) is unlikely. Therefore, we conclude that the initial increase of DBE is due to formation of C=O functional groups in the solution. The later decrease of DBE is due to molecule fragmentation, making compounds with smaller #C dominate in the latter stages of the photooxidation. To compensate this fragmentation effect, we introduce a novel molecular property, DBE to Carbon ratio (DBE/#C) which represents the average number of DBE associated with each carbon. The intensity-weighted average DBE/#C exhibited continuous increase (Fig. 6), approaching 1 by the end of the photooxidation experiment. Note that the the-

oretical maximum value of DBE/#C is 1. This observation indicates that a C=O double bond is associated with almost every carbon by the end of photooxidation.

Although DBE/#C alone cannot distinguish between C=O bonds in carbonyl and carboxylic acid functional groups, plotting OS_c against DBE/#C provides another dimension to the data analysis. This approach takes advantage of the fact that conversion of a carbonyl (i.e. aldehyde) to a carboxylic acid involves increase in the molecular OS_c, but the DBE/#C remains the same. OS_c is chosen instead of O/C here because O/C is affected by non-oxidative processes, such as hydration of aldehydes, while OS_c is not (Kroll et al., 2011). The trajectory of intensity-weighted average OS_c vs. DBE/#C is shown in Fig. 7, color coded by the illumination time. During the first 150 min of illumination, both OS_c and DBE/#C increase rapidly, leading to a dramatic and linear movement on the plot with a slope of 3. From 150 to 300 min of irradiation, the increases of OS_c and DBE/#C are both slower, but with OS_c increasing faster, leading to a slope of 4.3. During the last 150 min of irradiation, DBE/#C stays almost constant at 0.82, close to its theoretical maximum, while OS_c still exhibited slow but continuous increase. The slope during this time period is 9.

This observation is interpreted as observational evidence of poly-carbonyl intermediates rapidly forming in the solution during the early stages of photooxidation, giving rise to rapid increase in both DBE/#C and OS_c. As the illumination reaches 4 h, the average DBE/#C reaches 0.8, indicating that almost every carbon is associated with a C=O functional group at this moment. At the final stages of photooxidation, aldehyde-to-carboxylic acid conversion becomes dominant, leading to more increase in OS_c relative to DBE/#C. In addition to the intensity averaged trajectory, we also added representative compounds and major products detected during the photooxidation on the OS_c vs. DBE/#C plain (Fig. 7). Starting from levoglucosan at the left bottom corner, the major products sequentially formed during photooxidation are located towards the right upper corner of the plot. Oxalic acid, located at the right upper corner, presents the theoretical maximum for both DBE/#C and OS_c. The averaged trajectory passes through these major products.

3.2 Kinetic study

As mentioned in the experimental section, the kinetics of LG photooxidation was investigated under atmospherically relevant conditions, using DMSO as a reference compound. Both LG and DMSO decayed rapidly as soon as photooxidation was initiated. Typically, with 0.5 mM H_2O_2 in solution and over 30 min of illumination, LG decayed to 70 % of its starting value whereas DMSO decayed by approximately 80 % (Fig. 8a). Data were plotted in the form of Eq. (1), as illustrated in Fig. 8b for one run. Five experiments were performed to determine k^{II}_{LG} (Table 1) where the value of k^{II}_{DMSO}, $5.6 \times 10^9\,M^{-1}\,s^{-1}$, was taken to be the average of literature values (4.5×10^9 to $6.9 \times 10^9\,M^{-1}\,s^{-1}$ (Milne et al., 1989; Bardouki et al., 2002; Zhu et al., 2003). The concentration of H_2O_2 was varied between 0.5 and 1.5 M, but this variation did not affect the k^{II}_{LG} value obtained, consistent with the assumption that the concentration of OH is not of relevance to the relative rate method. The reproducibility of our experiments was excellent, and we report a value of $1.08 \pm 0.16 \times 10^9\,M^{-1}\,s^{-1}$, where the uncertainty reflects the standard deviation of the slope in the relative kinetic plot (Fig. 8b).

Hoffmann et al. (2010) have previously reported $2.4 \pm 0.3 \times 10^9\,M^{-1}\,s^{-1}$ at 298 K while Teraji and Arakaki (2010) have measured $1.6 \pm 0.3 \times 10^9\,M^{-1}\,s^{-1}$ at 303 K, pH 8. Although the k^{II}_{LG} value obtained from the current work is lower than previously reported, the agreement is reasonable considering the different methods employed. Hoffmann et al. (2010) used an excess amount of LG and monitored pseudo first order decay of OH radicals. Teraji and Arakaki (2010) also used an excess amount of LG, and calculated k^{II}_{LG} from the observed formation rate of a probe compound. This study is the first relative rate measurement, using direct measurement of LG.

3.3 Comparison with AMS data

Decay of LG was accompanied by a decay of f60 monitored by the AMS (Fig. 9a). The decay rate of f60 appears slower than that of LG, perhaps due to the fact that

compounds other than LG can also give rise to f60 in AMS. A simultaneous increase in f44 was also observed, indicating formation of oxygenated compounds such as organic acids, consistent with the proposed mechanisms mentioned above. The trend of decreasing f60 and increasing f44 closely resembles to that from field measurement of BB particles and heterogeneous oxidation of BB particles in the laboratory (Cubison et al., 2011; Ortega et al., 2013). Cubison et al. (2011) have demonstrated that the ratio of f44 to f60 changes in a non-linear manner, approaching a background level of f60 at 0.003, as the photochemical age of the BB air mass increases. Figure 9b demonstrates this trend from the compiled field data in Cubison et al. (2011). Overlain on this plot is the f44 to f60 trajectory obtained from the current work, color coded by the illumination time, which correlates nicely with field observations. This agreement is somewhat surprising given that the only reactive precursor is LG whereas BB particles in the environment contain a complex mixture of organic compounds. Oxidation of this complex and condensation of gas-phase organic acids could also contribute to an increase in f44. Nevertheless, the current work indicates that aqueous-phase photooxidation can qualitatively lead to similar observations as in the field, contributing to BB particle aging that arises from other mechanisms such as heterogeneous and gas-phase photooxidation.

4 Conclusions and environmental implications

This study presents the first detailed study of levoglucosan (LG) oxidation by OH radicals in the aqueous phase by online mass spectrometry: Aerosol Time of Flight Chemical Ionization Mass Spectrometry (Aerosol-ToF-CIMS). Being a soft ionization mass spectrometric technique, Aerosol-ToF-CIMS is extremely useful in elucidating the elemental composition of the reaction products, which shed light into fundamental chemistry of aqueous-phase photooxidation. This type of analysis is difficult to perform using hard ionization mass spectrometry.

Functionalization and bond-scission reactions were occurring simultaneously in the reaction system. While bond-scission reactions contributed to formation of smaller organic compounds, functionalization reactions gave rise to distinct trends of "+O" and "−2H" on mass defect plots. We propose that these trends have arisen from formation of hydroxyl and/or hydroperoxyl functional groups and conversion of hydroxyl to carbonyl functional groups, respectively. As a result, a compound with multiple hydroxyl functional groups, such as LG, can rapidly yield poly-carbonyl intermediates, representing a general reaction mechanism for polyols.

The current study introduces double bond equivalence to carbon ratio ($DB_c/\#C$) as a novel analysis framework for high resolution mass spectrometric data. It is particularly useful in photooxidation because DBE is most likely arising from formation of C=O in carbonyls and carboxylic acids. The degree of poly-carbonyl formation was observed to be extensive, leading to the average DBE/#C reaching 1 at the end of the photooxidation. As photooxidation proceeds further, these poly-carbonyl intermediates are converted into carboxylic acids, as is inferred from a OS_c to DBE/#C plot. This framework can be applied to other soft ionization mass spectrometric techniques with high mass resolution, providing functional group information.

From the kinetic experiments, the rate constant of LG reacting with OH radical was determined to be $1.08 \pm 0.16 \times 10^9\ M^{-1}\,s^{-1}$, indicating that LG loss due to aqueous-phase photooxidation can be significant, with a significant portion of LG lost during a typical lifetime of BB particles. This loss rate should be taken into account when LG is applied as a BB marker in chemical mass balance receptor models.

Using the AMS, simultaneous decay of f60 and increase in f44 were observed during LG aqueous oxidation, yielding behavior similar to that observed from field measurements. This observation qualitatively indicates that aqueous-phase photooxidation may be partially contributing to the observed decay of LG in the field and observed aging of BB particles.

Supplementary material related to this article is available online at http://www.atmos-chem-phys-discuss.net/14/8819/2014/acpd-14-8819-2014-supplement.pdf.

Acknowledgements. The authors thank NSERC for funding, Professor Jimenez for offering the field data, Aerodyne Inc. for technical support, and CFI for funding the purchase of the CIMS.

References

Aljawhary, D., Lee, A. K. Y., and Abbatt, J. P. D.: High-resolution chemical ionization mass spectrometry (ToF-CIMS): application to study SOA composition and processing, Atmos. Meas. Tech., 6, 3211–3224, doi:10.5194/amt-6-3211-2013, 2013. 8824, 8826

Allan, J., Delia, A., Coe, H., Bower, K., Alfarra, M., Jimenez, J., Middlebrook, A., Drewnick, F., Onasch, T., Canagaratna, M., Jayne, J., and Worsnop, D.: A generalised method for the extraction of chemically resolved mass spectra from aerodyne aerosol mass spectrometer data, J. Aerosol Sci., 35, 909–922, 2004. 8826

Bai, J., Sun, X., Zhang, C., Xu, Y., and Qi, C.: The OH-initiated atmospheric reaction mechanism and kinetics for levoglucosan emitted in biomass burning, Chemosphere, 93, 2004–2010, 2013. 8822

Bardouki, H., Rosa, M. B. D., Mihalopoulos, N., Palm, W.-U., and Zetzsch, C.: Kinetics and mechanism of the oxidation of dimethylsulfoxide (DMSO) and methanesulfinate (MSI^-) by OH radicals in aqueous medium, Atmos. Environ., 36, 4627–4634, 2002. 8833

Bateman, A. P., Nizkorodov, S. A., Laskin, J., and Laskin, A.: Photolytic processing of secondary organic aerosols dissolved in cloud droplets, Phys. Chem. Chem. Phys., 13, 12199–12212, 2011. 8831

Bertram, T. H., Kimmel, J. R., Crisp, T. A., Ryder, O. S., Yatavelli, R. L. N., Thornton, J. A., Cubison, M. J., Gonin, M., and Worsnop, D. R.: A field-deployable, chemical ionization time-of-flight mass spectrometer, Atmos. Meas. Tech., 4, 1471–1479, doi:10.5194/amt-4-1471-2011, 2011. 8824

Blando, J. D. and Turpin, B. J.: Secondary organic aerosol formation in cloud and fog droplets: a literature evaluation of plausibility, Atmos. Environ., 34, 1623–1632, 2000. 8822

Canagaratna, M. R., Jayne, J. T., Jimenez, J. L., Allan, J. D., Alfarra, M. R., Zhang, Q., Onasch, T. B., Drewnick, F., Coe, H., Middlebrook, A., Delia, A., Williams, L. R., Trimborn, A. M., Northway, M. J., DeCarlo, P. F., Kolb, C. E., Davidovits, P., and Worsnop, D. R.: Chemical and microphysical characterization of ambient aerosols with the aerodyne aerosol mass spectrometer, Mass Spectrom. Rev., 26, 185–222, 2007. 8826

Cubison, M. J., Ortega, A. M., Hayes, P. L., Farmer, D. K., Day, D., Lechner, M. J., Brune, W. H., Apel, E., Diskin, G. S., Fisher, J. A., Fuelberg, H. E., Hecobian, A., Knapp, D. J., Mikoviny, T., Riemer, D., Sachse, G. W., Sessions, W., Weber, R. J., Weinheimer, A. J., Wisthaler, A., and Jimenez, J. L.: Effects of aging on organic aerosol from open biomass burning smoke in aircraft and laboratory studies, Atmos. Chem. Phys., 11, 12049–12064, doi:10.5194/acp-11-12049-2011, 2011. 8821, 8834, 8850

Ervens, B., Turpin, B. J., and Weber, R. J.: Secondary organic aerosol formation in cloud droplets and aqueous particles (aqSOA): a review of laboratory, field and model studies, Atmos. Chem. Phys., 11, 11069–11102, doi:10.5194/acp-11-11069-2011, 2011. 8822

Fraser, M. and Lakshmanan, K.: Using levoglucosan as a molecular marker for the long-range transport of biomass combustion aerosols, Environ. Sci. Technol., 34, 4560–4564, 2000. 8821

Grieshop, A. P., Donahue, N. M., and Robinson, A. L.: Laboratory investigation of photochemical oxidation of organic aerosol from wood fires 2: analysis of aerosol mass spectrometer data, Atmos. Chem. Phys., 9, 2227–2240, doi:10.5194/acp-9-2227-2009, 2009. 8821

Hearn, J. D. and Smith, G. D.: A chemical ionization mass spectrometry method for the online analysis of organic aerosols, Anal. Chem., 76, 2820–2826, 2004. 8823

Hennigan, C. J., Sullivan, A. P., Collett, J. L., and Robinson, A. L.: Levoglucosan stability in biomass burning particles exposed to hydroxyl radicals, Geophys. Res. Lett., 37, L09806, doi:10.1029/2010GL043088, 2010. 8821

Hoffmann, D., Tilgner, A., Iinuma, Y., and Herrmann, H.: Atmospheric stability of levoglucosan: a detailed laboratory and modeling study, Environ. Sci. Technol., 44, 694–699, 2010. 8822

Holmes, B. J. and Petrucci, G. A.: Water-soluble oligomer formation from acid-catalyzed reactions of levoglucosan in proxies of atmospheric aqueous aerosols, Environ. Sci. Technol., 40, 4983–4989, 2006. 8822

Holmes, B. J. and Petrucci, G. A.: Oligomerization of levoglucosan by Fenton chemistry in proxies of biomass burning aerosols, J. Atmos. Chem., 58, 151–166, 2007. 8822

Hughey, C. A., Hendrickson, C. L., Rodgers, R. P., Marshall, A. G., and Qian, K.: Kendrick mass defect spectrum: A compact visual analysis for ultrahigh-resolution broadband mass spectra, Anal. Chem., 73, 4676–4681, 2001. 8827

Jacob, D.: Chemistry of OH in remote clouds and its role in the production of formic-acid peroxymonosulfate, J. Geophys. Res. Atmos., 91, 9807–9826, 1986. 8825

Jimenez, J. L., Canagaratna, M. R., Donahue, N. M., Prevot, A. S. H., Zhang, Q., Kroll, J. H., DeCarlo, P. F., Allan, J. D., Coe, H., Ng, N. L., Aiken, A. C., Docherty, K. S., Ulbrich, I. M., Grieshop, A. P., Robinson, A. L., Duplissy, J., Smith, J. D., Wilson, K. R., Lanz, V. A., Hueglin, C., Sun, Y. L., Tian, J., Laaksonen, A., Raatikainen, T., Rautiainen, J., Vaattovaara, P., Ehn, M., Kulmala, M., Tomlinson, J. M., Collins, D. R., Cubison, M. J., Dunlea, E. J., Huffman, J. A., Onasch, T. B., Alfarra, M. R., Williams, P. I., Bower, K., Kondo, Y., Schneider, J., Drewnick, F., Borrmann, S., Weimer, S., Demerjian, K., Salcedo, D., Cottrell, L., Griffin, R., Takami, A., Miyoshi, T., Hatakeyama, S., Shimono, A., Sun, J. Y., Zhang, Y. M., Dzepina, K., Kimmel, J. R., Sueper, D., Jayne, J. T., Herndon, S. C., Trimborn, A. M., Williams, L. R., Wood, E. C., Middlebrook, A. M., Kolb, C. E., Baltensperger, U., and Worsnop, D. R.: Evolution of organic aerosols in the atmosphere, Science, 326, 1525–1529, 2009. 8821

Kessler, S. H., Smith, J. D., Che, D. L., Worsnop, D. R., Wilson, K. R., and Kroll, J. H.: Chemical sinks of organic aerosol: kinetics and products of the heterogeneous oxidation of erythritol and levoglucosan, Environ. Sci. Technol., 44, 7005–7010, 2010. 8821

Knopf, D. A., Forrester, S. M., and Slade, J. H.: Heterogeneous oxidation kinetics of organic biomass burning aerosol surrogates by O_3, NO_2, N_2O_5, and NO_3, Phys. Chem. Chem. Phys., 13, 21050–21062, 2011. 8821

Kroll, J. H., Donahue, N. M., Jimenez, J. L., Kessler, S. H., Canagaratna, M. R., Wilson, K. R., Altieri, K. E., Mazzoleni, L. R., Wozniak, A. S., Bluhm, H., Mysak, E. R., Smith, J. D., Kolb, C. E., and Worsnop, D. R.: Carbon oxidation state as a metric for describing the chemistry of atmospheric organic aerosol, Nat. Chem., 3, 133–139, 2011. 8831

Lee, A. K. Y., Zhao, R., Gao, S. S., and Abbatt, J. P. D.: Aqueous-phase OH oxidation of glyoxal: application of a novel analytical approach employing aerosol mass spectrometry and complementary off-line techniques, J. Phys. Chem. A, 115, 10517–10526, 2011. 8826, 8830

Lee, A. K. Y., Hayden, K. L., Herckes, P., Leaitch, W. R., Liggio, J., Macdonald, A. M., and Abbatt, J. P. D.: Characterization of aerosol and cloud water at a mountain site during

WACS 2010: secondary organic aerosol formation through oxidative cloud processing, Atmos. Chem. Phys., 12, 7103–7116, doi:10.5194/acp-12-7103-2012, 2012. 8826
Lim, Y. B., Tan, Y., Perri, M. J., Seitzinger, S. P., and Turpin, B. J.: Aqueous chemistry and its role in secondary organic aerosol (SOA) formation, Atmos. Chem. Phys., 10, 10521–10539, doi:10.5194/acp-10-10521-2010, 2010. 8826, 8830
May, A. A., Saleh, R., Hennigan, C. J., Donahue, N. M., and Robinson, A. L.: Volatility of organic molecular markers used for source apportionment analysis: measurements and implications for atmospheric lifetime, Environ. Sci. Technol., 46, 12435–12444, 2012. 8821
Milne, P. J., Zika, R. G., and Saltzman, E. S.: Biogenic Sulfur in the Environment, American Chemical Society, Washington DC, 1989. 8833
Mochida, M., Kawamura, K., Fu, P., and Takemura, T.: Seasonal variation of levoglucosan in aerosols over the western North Pacific and its assessment as a biomass-burning tracer, Atmos. Environ., 44, 3511–3518, 2010. 8821
Ortega, A. M., Day, D. A., Cubison, M. J., Brune, W. H., Bon, D., de Gouw, J. A., and Jimenez, J. L.: Secondary organic aerosol formation and primary organic aerosol oxidation from biomass-burning smoke in a flow reactor during FLAME-3, Atmos. Chem. Phys., 13, 11551–11571, doi:10.5194/acp-13-11551-2013, 2013. 8821, 8834
Petters, M. D. and Kreidenweis, S. M.: A single parameter representation of hygroscopic growth and cloud condensation nucleus activity, Atmos. Chem. Phys., 7, 1961–1971, doi:10.5194/acp-7-1961-2007, 2007. 8822
Petters, M. D., Carrico, C. M., Kreidenweis, S. M., Prenni, A. J., DeMott, P. J., Collett, J. L., and Moosmuller, H.: Cloud condensation nucleation activity of biomass burning aerosol, J. Geophys. Res.-Atmos., 114, D22205, doi:10.1029/2009JD012353, 2009. 8822
Robinson, A. L., Subramanian, R., Donahue, N. M., Bernardo-Bricker, A., and Rogge, W. F.: Source apportionment of molecular markers and organic aerosol, 2. Biomass smoke, Environ. Sci. Technol., 40, 7811–7819, 2006. 8821
Saarikoski, S., Timonen, H., Saarnio, K., Aurela, M., Järvi, L., Keronen, P., Kerminen, V.-M., and Hillamo, R.: Sources of organic carbon in fine particulate matter in northern European urban air, Atmos. Chem. Phys., 8, 6281–6295, doi:10.5194/acp-8-6281-2008, 2008. 8821
Sareen, N., Schwier, A. N., Shapiro, E. L., Mitroo, D., and McNeill, V. F.: Secondary organic material formed by methylglyoxal in aqueous aerosol mimics, Atmos. Chem. Phys., 10, 997–1016, doi:10.5194/acp-10-997-2010, 2010. 8824

Schauer, J., Rogge, W., Hildemann, L., Mazurek, M., Cass, G., and Simoneit, B.: Source apportionment of airborne particulate matter using organic compounds as tracers, Atmos. Environ., 30, 3837–3855, 1996. 8821
Schuchmann, M. N. and von Sonntag, C.: The rapid hydration of the acetyl radical – a pulse radiolosys study of acetaldehyde in aqueous-solution, J. Am. Chem. Soc., 110, 5698–5701, 1988. 8830
Simoneit, B. R. T.: Biomass burning – a review of organic tracers for smoke from incomplete combustion, Appl. Geochem., 17, 129–162, 2002. 8821
Simoneit, B. R. T., Schauer, J. J., Nolte, C. G., Oros, D. R., Elias, V. O., Fraser, M. P., Rogge, W. F., and Cass, G. R.: Levoglucosan, a tracer for cellulose in biomass burning and atmospheric particles, Atmos. Environ., 33, 173–182, 1999. 8821
Simoneit, B. R. T., Elias, V. O., Kobayashi, M., Kawamura, K., Rushdi, A. I., Medeiros, P. M., Rogge, W. F., and Didyk, B. M.: Sugars – dominant water-soluble organic compounds in soils and characterization as tracers in atmospheric particulate matter, Environ. Sci. Technol., 38, 5939–5949, 2004. 8821
Teraji, T. and Arakaki, T.: Bimolecular rate constants between levoglucosan and hydroxyl radical: effects of pH and temperature, Chem. Lett., 39, 900–901, 2010. 8822
von Sonntag, C., Dowideit, P., Fang, X., Mertens, R., Pan, X., Schuchmann, M. N., and Schuchmann, H.-P.: The fate of peroxyl radicals in aqueous solution, Water Sci. Technol., 35, 9–15, 1997. 8828
Zhang, X., Hecobian, A., Zheng, M., Frank, N. H., and Weber, R. J.: Biomass burning impact on $PM_{2.5}$ over the southeastern US during 2007: integrating chemically speciated FRM filter measurements, MODIS fire counts and PMF analysis, Atmos. Chem. Phys., 10, 6839–6853, doi:10.5194/acp-10-6839-2010, 2010. 8821
Zhao, R., Lee, A. K. Y., and Abbatt, J. P. D.: Investigation of aqueous-phase photooxidation of glyoxal and methylglyoxal by aerosol chemical ionization mass spectrometry: observation of hydroxyhydroperoxide formation, J. Phys. Chem. A, 116, 6253–6263, 2012. 8824, 8826, 8830
Zhu, L., Nicovich, J. M., and Wine, P. H.: Temperature-dependent kinetics studies of aqueous phase reactions of hydroxyl radicals with dimethylsulfoxide, dimethylsulfone, and methanesulfonate, Aquat. Sci., 65, 425–435, 2003. 8833

Table 1. Summary of the conditions and the results of the kinetic experiments.

Exp. #	[LG] (μM)	[DMSO] (μM)	H_2O_2 (μM)	k^{II}_{LG} ($M^{-1}s^{-1}$)
1	30	5	0.5	8.06×10^8
2	30	5	1	1.10×10^9
3	30	5	1	1.08×10^9
4	30	5	1.5	1.23×10^9
5	30	5	0.5	1.16×10^9
			Average	1.08×10^9

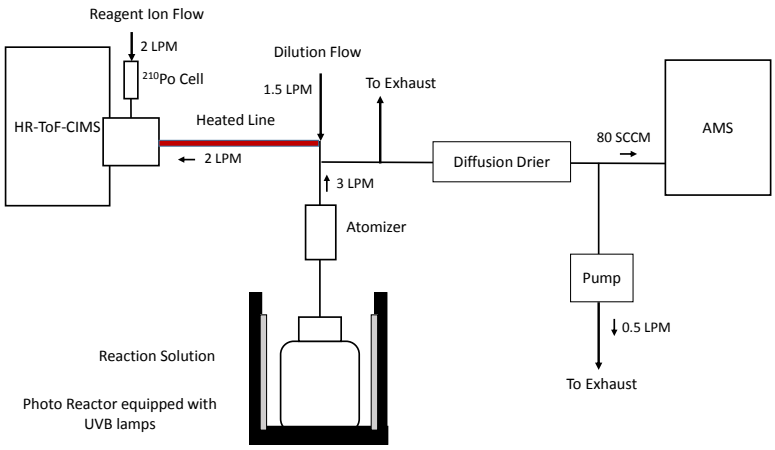

Fig. 1. The experimental apparatus.

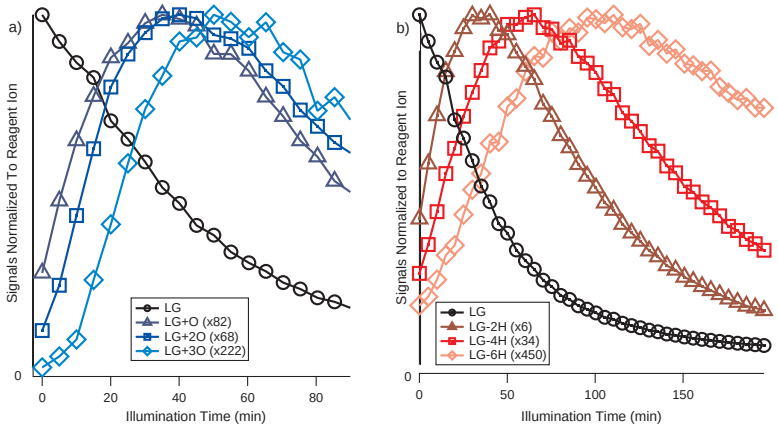

Fig. 2. The evolution of the "+O" **(a)** and the "−2H" **(b)** series from levoglucosan (LG). The signal of each compound normalized by the reagent ion intensity at m/z 145 ($I(H_2O)^-$) is shown as a function of the irradiation time. The signals are multiplied by the bracketed number to be on scale.

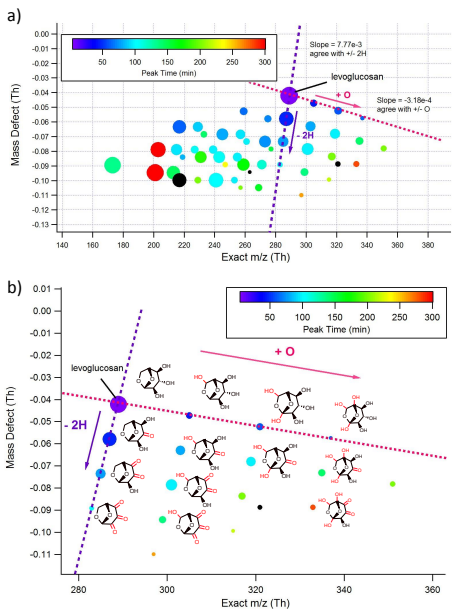

Fig. 3. The mass defect diagram of the major products detected using the iodide water cluster ($I(H_2O)_n^-$) reagent ion **(a)**. The color code indicates the time at which each compound reached its maximum signal intensity and the area of the circles represents the maximum signal intensity reached (in log scale). Compounds that did not reach their maxima during the first 300 min of illumination are shown in black. The +O and the −2H series fall on the slope indicated by the dotted lines. The region relevant to products arising from +O and −2H trends is presented in **(b)**. The proposed structures of each product are shown beside the data points.

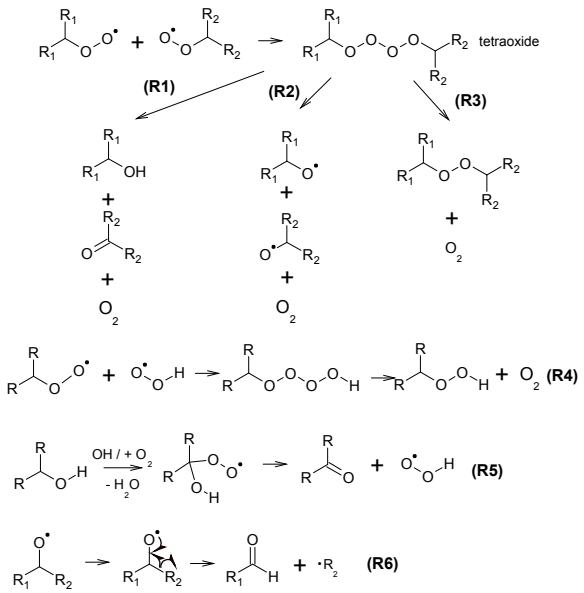

Fig. 4. Sample reaction mechanisms that give rise to the +O and −2H trends. The tetraoxide intermediate forming from two alkylperoxy radicals can result in a variety of products as shown in (R1) to (R3), among which (R1) can lead to formation of the hydroxyl functional group. A hydroperoxy functional group can be formed from RO_2 + HO_2 (R4). The hydroxyl-to-carbonyl conversion shown in (R5) is likely responsible for the −2H trend. Alkoxy radicals trigger bond-session reactions and give rise to an aldehydic compound (R6).

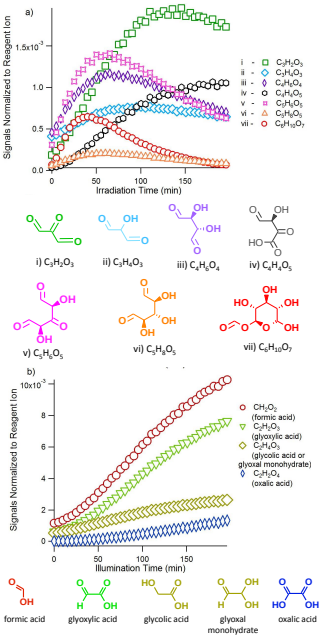

Fig. 5. Evolution of chain scission products measured by the $I(H_2O)_n^-$ reagent ion. Selected major products with three to six carbons are shown in **(a)**, with their proposed structures. The proposed reaction mechanisms leading to their formation are attached in Fig. S1. Formation of small organic acids with one or two carbons are shown in **(b)**. All the signals have been normalized against the reagent ion ($I(H_2O)^-$) at m/z 145.

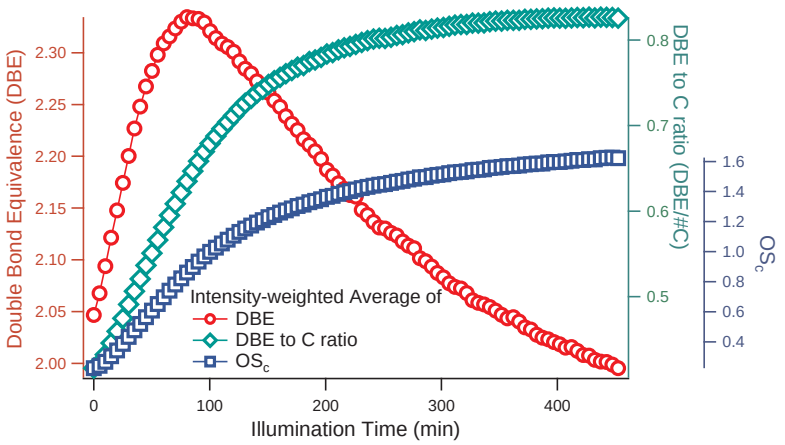

Fig. 6. Intensity-weighted average of double bond equivalence (DBE), DBE to carbon ratio (DBE/#C) and oxidation state (OS_c) as a function of irradiation time.

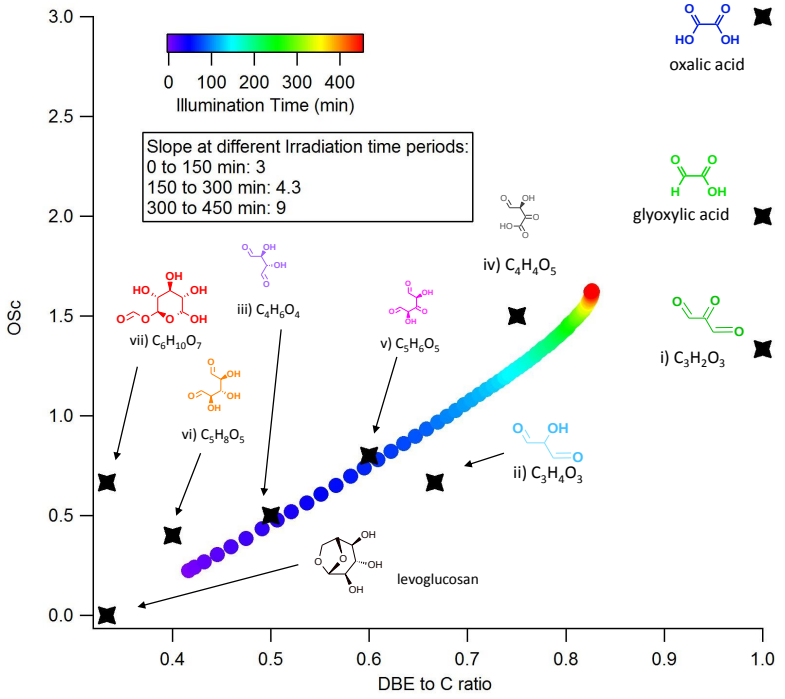

Fig. 7. OS_c vs. DBE/#C plot. The intensity-weighted average OS_c and DBE/#C from the products listed in Table S1 are displayed here. The color code represents the illumination time. The coordinates of major compounds are also shown.

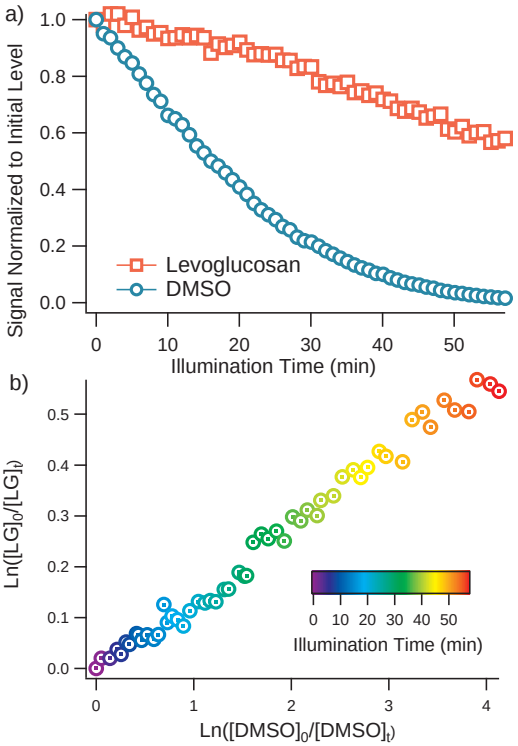

Fig. 8. The time series of LG and DMSO during a kinetic experiment (Exp. #1 in Table 1) are shown in **(a)**. The signals are normalized to that at the beginning of the photooxidation. The relative kinetics plot from the same experiment is shown in **(b)** according to Eq. (1). The color code indicates the illumination time.

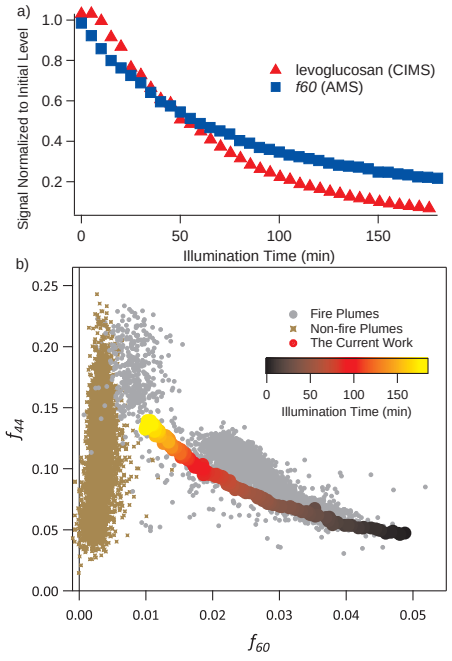

Fig. 9. The decay of levoglucosan monitored by the Aerosol-ToF-CIMS and the decay of f60 monitored by the AMS **(a)**, and the f60 vs. f40 trajectory from the current work compared to field measurements **(b)**. The trajectory obtained in the current work is color coded with irradiation time. The compiled data (Cubison et al., 2011) from field measurements in fire plumes (grey) and non-fire plumes (brown) are also shown.